BLANK PAGE

Scientific Report No. 1
Contract N140(70024)75686B
June 1964

• applied • mathematics •

Acoustic Radiation from a Finite Cylinder - Numerical Results

by

PML Staff

for

U. S. Navy Underwater Sound Laboratory

PARKE MATHEMATICAL LABORATORIES, Inc.
One River Road • Carlisle, Massachusetts

PARKE MATHEMATICAL LABORATORIES, INCORPORATED
ONE RIVER ROAD • CARLISLE, MASSACHUSETTS

Requests for additional copies by Agencies of the Department of Defense, their contractors, and other Government agencies should be directed to the:

DEFENSE DOCUMENTATION CENTER (DDC)
CAMERON STATION
ALEXANDRIA, VIRGINIA

Department of Defense contractors must be established for DDC services or have their 'need-to-know' certified by the cognizant military agency of their project or contract.

All other persons and organizations should apply to the:

U.S. DEPARTMENT OF COMMERCE
OFFICE OF TECHNICAL SERVICES
WASHINGTON 25, D.C.

A limited number of copies are also available by writing to:

PARKE MATHEMATICAL LABORATORIES, INC.
ONE RIVER ROAD
CARLISLE, MASSACHUSETTS

Scientific Report No. 1

Contract N140(70024)75686L

June 1964

• a p p l i e d • m a t h e m a t i c s • •

Acoustic Radiation from a Finite Cylinder - Numerical Results

by

PML Staff

for

U. S. Navy Underwater Sound Laboratory

PARKE MATHEMATICAL LABORATORIES, Inc.
One River Road • Carlisle, Massachusetts

SCIENTIFIC REPORTS

their purpose and place

...A·P·P·L·I·E·D··M·A·T·H·E·M·A·T·I·C·I·A·N·S...

THE EVER INCREASING NEED TO BE INFORMED has caused an ever increasing volume of publications. The very quantity of these publications, however, makes it difficult to satisfy the need, because it becomes more and more arduous to locate the literature pertinent to any one subject; and because any one of us becomes more and more weary of having so much to read. Moreover, only a small minority of these publications may help satisfy the need, because an overwhelming majority is void of content.

Consequently, it is imperative to present to the public only manuscripts which do carry new information without undue verbiage; hoping to be judged not by the number of published pages but by their quality. In particular, papers in the field of Applied Mathematics ought to be published only if they contain one or more of the following items: new basic results, new methods, new applications, new numerical results, new presentation of difficult and important topics, up-to-date bibliographies; and if the number of their pages is not dictated by the desire of imposing upon the superficial reader.

To discharge our contractual obligations, we publish *Technical or Scientific Reports*, such as the one you now have in your hands. It has been our constant policy to see to it, that they satisfy the above strict criterion.

PARKE MATHEMATICAL LABORATORIES, INC.
carlisle, massachusetts

Table of Contents

BLANK PAGE

Acoustic Radiation from a Finite Cylinder - Numerical Results

by

PML Staff

Introduction

In an earlier report we presented an approximate method for calculating the sound field of a cylinder of finite length.[1] In this method the field, which can be represented exactly by an infinite series expansion in terms of spherical wave functions, is approximated instead by the finite series

$$\psi(r,\theta) = \sum_{n=0}^{N} a_n h_n(kr) P_n(\cos\theta), \qquad (1)$$

for the axially symmetric case to be considered. The complex coefficients a_n are determined by fitting them to the given boundary conditions through a weighted least squares analysis. A spherical coordinate system (see Fig.1) with origin at the center of the cylinder and polar axis along the cylinder axis is employed.

The method does not differ fundamentally from the standard one which would be used for radiation from a sphere. The normal derivative of ψ is calculated on the surface of the cylinder and equated to the specified normal velocity of the cylinder surface which leads to relationships from which the coefficients can be determined. But the fact that the surface in question is not a constant coordinate surface greatly complicates the computations and obscures the similarity with familiar problems. Although

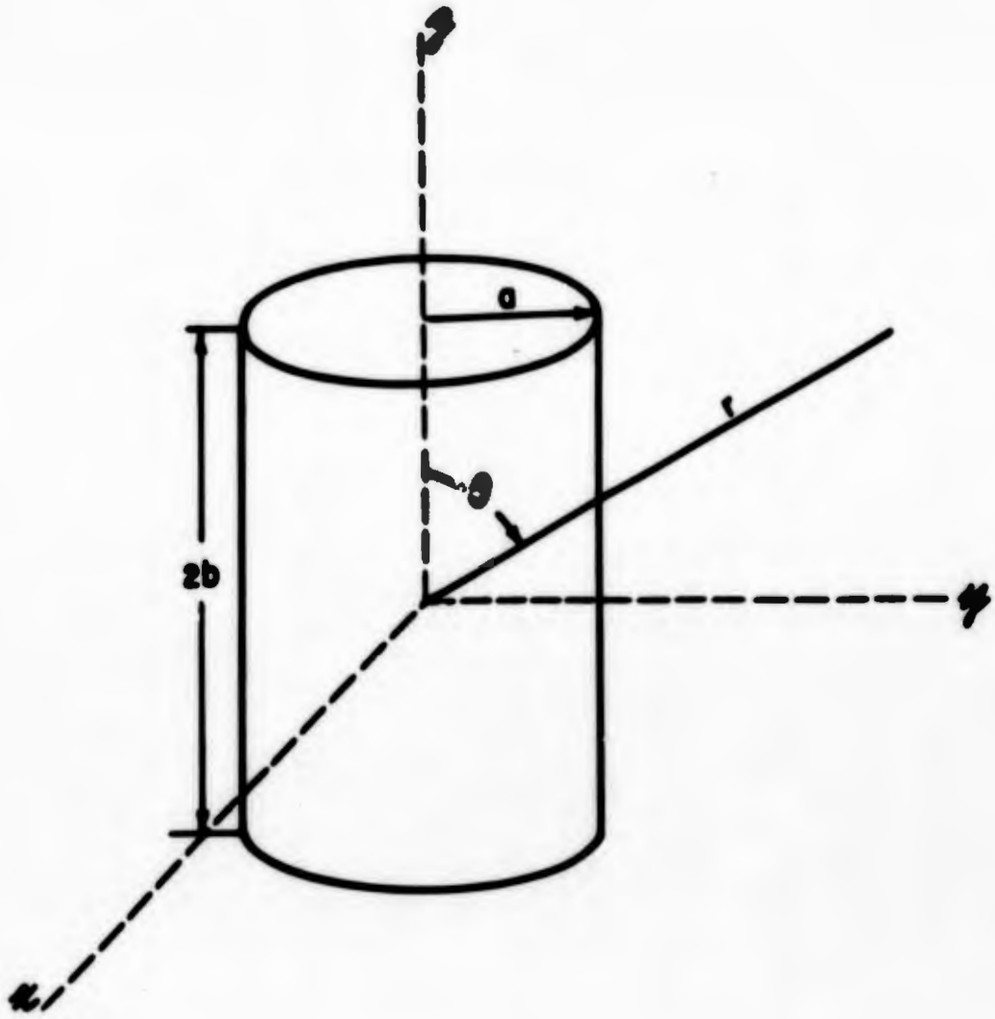

Fig. 1 Coordinates and dimensions for finite cylinder calculation.

this complication is a genuine one from the standpoint of making practical computations, it can be overcome as the results in this report will demonstrate. As compared to other methods described in the literature[2,3,4] this method is conceptually simpler and less dependent on those kinds of approximations and assumptions which are difficult to evaluate. Although these are important advantages it is clear that in the final analysis any method for calculating acoustic radiation from objects such as a finite cylinder stands or falls on its ability to provide numerical results of sufficient accuracy for practical purposes. Therefore we regard the results to be presented here, which go beyond any results obtained by other methods, as the chief indication of the value of the present method.

For cylinder sizes which exceed the wave length hand computations became impractical, and a computer program was written for determining the coefficients[5]. Computations were performed on IBM 7090 and IBM 7094 computers, and the purpose of this report is to present these results for the coefficients as well as various physically meaningful results which have been calculated with these coefficients. The existing program is not efficient enough to determine as many coefficients as are needed for calculating all aspects of the sound field in all cases. Although there are several ways in which the efficiency of the program can be improved the machine runs were stopped when enough coefficients had been obtained to provide a reasonable evaluation of the results.

The computer program was written for the case of axially symmetric vibration of a cylinder of finite length. However, the method is not

confined to the axially symmetric case, nor is it confined to cylinders. The method can be used for any reasonable velocity distribution on any body which is topologically equivalent to a sphere.

The Expansion Coefficients

The height of the cylinder is $2b$ and the radius is a as shown in Fig. 1. We have obtained expansion coefficients for three different cases: $ka = 1, 2$ and 5, all with $b/a = 2$. The boundary condition imposed in all cases is that for which the ends of the cylinder are motionless and the sides are vibrating radially with the uniform normal velocity $Ue^{-i\omega t}$. This boundary condition is axially symmetric, and it is also symmetric about the equatorial plane which makes the odd order coefficients zero.

For given N there are, in these cases, $N/2 + 1$ coefficients. The number of terms required for an adequate approximation is one of the questions which must be investigated. It must be remembered that all the coefficients have different values for each value of N, although for $n \ll N$ a_n converges to a stable value as N increases. For the case $ka = 5$, $kb = 10$ the coefficients were calculated for many different values of N in order to show this aspect of the situation in detail. The results for this case are given in Table 1 for $N = 4, 6, 8, \ldots, 20$ where the numbers given are the dimensionless ratio a_n/aU. Table 1 shows clearly, for example, that a_0 has reached an approximately stable value at $N = 20$, while a_{10} is still varying considerably at $N = 20$, and that the single value obtained for a_{20} cannot be regarded as a usable approximation. This means that the coefficients obtained for $N = 20$ can only be used to calculate quantities for

which the series converges before $n = 20$ and for which the inaccurate higher order coefficients are not required.

In Table 2 we give the coefficients for the case $ka = 2$, $kb = 4$ with $N = 10, 12$ and in Table 3 for the case $ka = 1$, $kb = 2$ with $N = 6, 8$. Note that a_n for fixed n varies rapidly with ka. It would not be possible from the results for these three ka values to make useful estimates of a_n for intermediate values of ka.

Far Field Patterns

By using the asymptotic form of the spherical Hankel function in Eqn.(1) we obtain for the pressure in the far field

$$p(r,\theta) = i k \rho c \psi(r,\theta) = k a \rho c U \frac{e^{ikr}}{kr} \sum_{n=0}^{N} \frac{a_n}{a U} i^{-n} P_n(\cos\theta). \qquad (2)$$

The magnitude and phase of the sum in Eqn.(2) was calculated as a function of θ using the coefficients in Tables 1-3 for the maximum value of N. The magnitude was normalized to unity at $\theta = 90^\circ$ (the direction perpendicular to the cylinder axis), and the results are shown in Figures 2-7 where each finite cylinder case is compared with a line source of length $2b$ and with a radially vibrating band of length $2b$ on an infinite rigid cylinder of radius a. The expression for the far field pressure of the band source on the infinite cylinder was obtained from the work of Laird and Cohen[6], and, in our notation, is

$$p(r,\theta) = \frac{2\rho c U kb}{\pi} \frac{e^{ikr}}{kr} \frac{\sin(kb\cos\theta)}{kb\cos\theta} \frac{1}{\sin\theta\, H_0'(ka\sin\theta)}, \qquad (3)$$

Table 1

Real and Imaginary Parts of $\frac{a_n}{\Sigma U}$

$ka = 5 \quad kb = 10$

N \ n	0	2	4	6	8	10	12	14	16	18	20
4	4.30220×10^{-1} $+1.36804 \times 10^{-1} i$	1.49906 $+6.02216 \times 10^{-1} i$	2.02783 $+1.00787 i$								
6	4.51596×10^{-1} $+2.14600 \times 10^{-1} i$	1.37756 $+4.89487 \times 10^{-1} i$	2.17080 $+1.10696 i$	2.1944 $+5.65554 \times 10^{-1} i$							
8	4.61319×10^{-1} $+2.37628 \times 10^{-1} i$	1.35480 $+4.84171 \times 10^{-1} i$	2.03056 $+1.05154 i$	2.00445 $+9.72810 \times 10^{-1} i$	2.34789×10^{-1} $+1.14009 \times 10^{-1} i$						
10	4.62848×10^{-1} $+2.45814 \times 10^{-1} i$	1.36713 $+4.12135 \times 10^{-1} i$	1.90609 $+9.89121 \times 10^{-1} i$	2.36531 $+1.15650 i$	5.40217×10^{-1} $+2.72329 \times 10^{-1} i$	2.52037×10^{-2} $+1.29498 \times 10^{-2} i$					
12	4.61496×10^{-1} $+2.45174 \times 10^{-1} i$	1.38567 $+4.00068 \times 10^{-1} i$	1.83146 $+9.99828 \times 10^{-1} i$	2.40512 $+1.21919 i$	8.45987×10^{-1} $+4.40416 \times 10^{-1} i$	7.75671×10^{-2} $+4.21063 \times 10^{-2} i$	1.88176×10^{-3} $+1.02062 \times 10^{-3} i$				
14	4.57606×10^{-1} $+2.41062 \times 10^{-1} i$	1.39996 $+4.49969 \times 10^{-1} i$	1.79366 $+9.08576 \times 10^{-1} i$	2.47422 $+1.21774 i$	1.11899 $+6.02844 \times 10^{-1} i$	1.52394×10^{-1} $+8.60659 \times 10^{-2} i$	7.07456×10^{-3} $+4.15171 \times 10^{-3} i$	9.72173×10^{-5} $+5.91158 \times 10^{-5} i$			
16	4.50161×10^{-1} $+2.35634 \times 10^{-1} i$	1.40990 $+4.67881 \times 10^{-1} i$	1.77995 $+8.93482 \times 10^{-1} i$	2.44924 $+1.18306 i$	1.34816 $+7.44988 \times 10^{-1} i$	2.41770×10^{-1} $+1.42655 \times 10^{-1} i$	1.65278×10^{-2} $+1.00691 \times 10^{-2} i$	4.44274×10^{-4} $+2.75295 \times 10^{-4} i$	3.87062×10^{-6} $+2.42848 \times 10^{-6} i$		
18	4.57176×10^{-1} $+2.30373 \times 10^{-1} i$	1.41533 $+4.34870 \times 10^{-1} i$	1.78039 $+8.84469 \times 10^{-1} i$	2.38710 $+1.13901 i$	1.52633 $+8.55657 \times 10^{-1} i$	3.35781×10^{-1} $+2.01738 \times 10^{-1} i$	2.99667×10^{-2} $+1.85291 \times 10^{-2} i$	1.19029×10^{-3} $+7.38977 \times 10^{-4} i$	2.00812×10^{-5} $+1.26380 \times 10^{-5} i$	1.19218×10^{-7} $+7.45169 \times 10^{-8} i$	
20	4.53671×10^{-1} $+2.26467 \times 10^{-1} i$	1.41755 $+5.07957 \times 10^{-1} i$	1.78751 $+8.85411 \times 10^{-1} i$	2.32796 $+1.09744 i$	1.65310 $+9.36879 \times 10^{-1} i$	4.45133×10^{-1} $+2.55738 \times 10^{-1} i$	4.62602×10^{-2} $+2.84081 \times 10^{-2} i$	2.36779×10^{-3} $+1.46037 \times 10^{-3} i$	5.30949×10^{-5} $+3.62332 \times 10^{-5} i$	6.75849×10^{-7} $+4.13648 \times 10^{-7} i$	2.81496×10^{-9} $+1.71833 \times 10^{-9} i$

PARKE MATHEMATICAL LABORATORIES, INCORPORATED
BEDFORD ROAD • CARLISLE, MASSACHUSETTS

Table 2

m \ n	0	2	4	6	8	10	12
10	-9.68605×10^{-1} $-2.59532 \times 10^{-1} i$	-1.68678 $-5.14836 \times 10^{-1} i$	-3.73213×10^{-1} $-5.79457 \times 10^{-2} i$	-1.99896×10^{-2} $-4.21461 \times 10^{-4} i$	-3.22904×10^{-4} $+2.68568 \times 10^{-5} i$	-1.41851×10^{-6} $+2.26648 \times 10^{-7} i$	
12	-9.69585×10^{-1} $-2.59621 \times 10^{-1} i$	-1.68708 $-5.14497 \times 10^{-1} i$	-3.74795×10^{-1} $-5.70284 \times 10^{-2} i$	-2.02396×10^{-2} $-2.82479 \times 10^{-4} i$	-3.32672×10^{-4} $+3.17179 \times 10^{-5} i$	-1.53929×10^{-6} $+2.92507 \times 10^{-7} i$	-4.21595×10^{-10} $+2.29737 \times 10^{-10} i$

Real and Imaginary Parts of $\frac{a_n}{2U}$

$ka = 2$ $kb = 4$

PARKE MATHEMATICAL LABORATORIES, INCORPORATED
ONE RIVER ROAD • CARLISLE, MASSACHUSETTS

Table 3

Real and Imaginary Parts of $\frac{a_n}{aU}$

$k_2 = 1 \quad k_b = 2$

N \ n	0	2	4	6	8
6	-4.14275×10^{-1} $-1.02662\,i$	-1.83199×10^{-1} $-3.25002 \times 10^{-1}\,i$	-5.39644×10^{-3} $-7.63600 \times 10^{-3}\,i$	-2.57625×10^{-5} -3.10759×10^{-5}	
8	-4.15254×10^{-1} $-1.03028\,i$	-2.18263×10^{-1} $-3.47305 \times 10^{-1}\,i$	-8.80648×10^{-3} $-9.80149 \times 10^{-3}\,i$	-7.76692×10^{-5} $-6.40892 \times 10^{-5}\,i$	-1.58124×10^{-7} $-1.00642 \times 10^{-7}\,i$

BLANK PAGE

BLANK PAGE

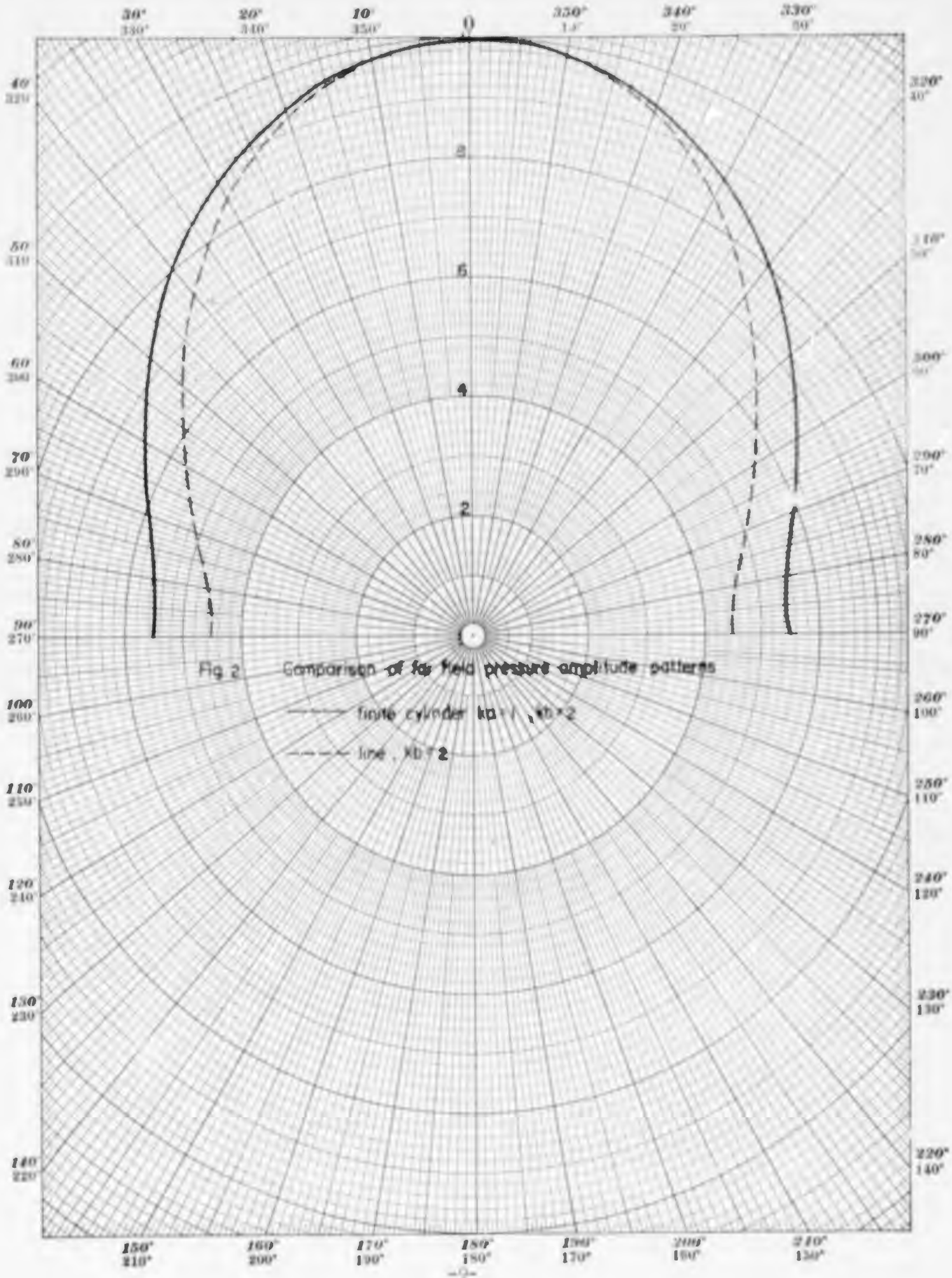

Fig 2 Comparison of far field pressure amplitude patterns

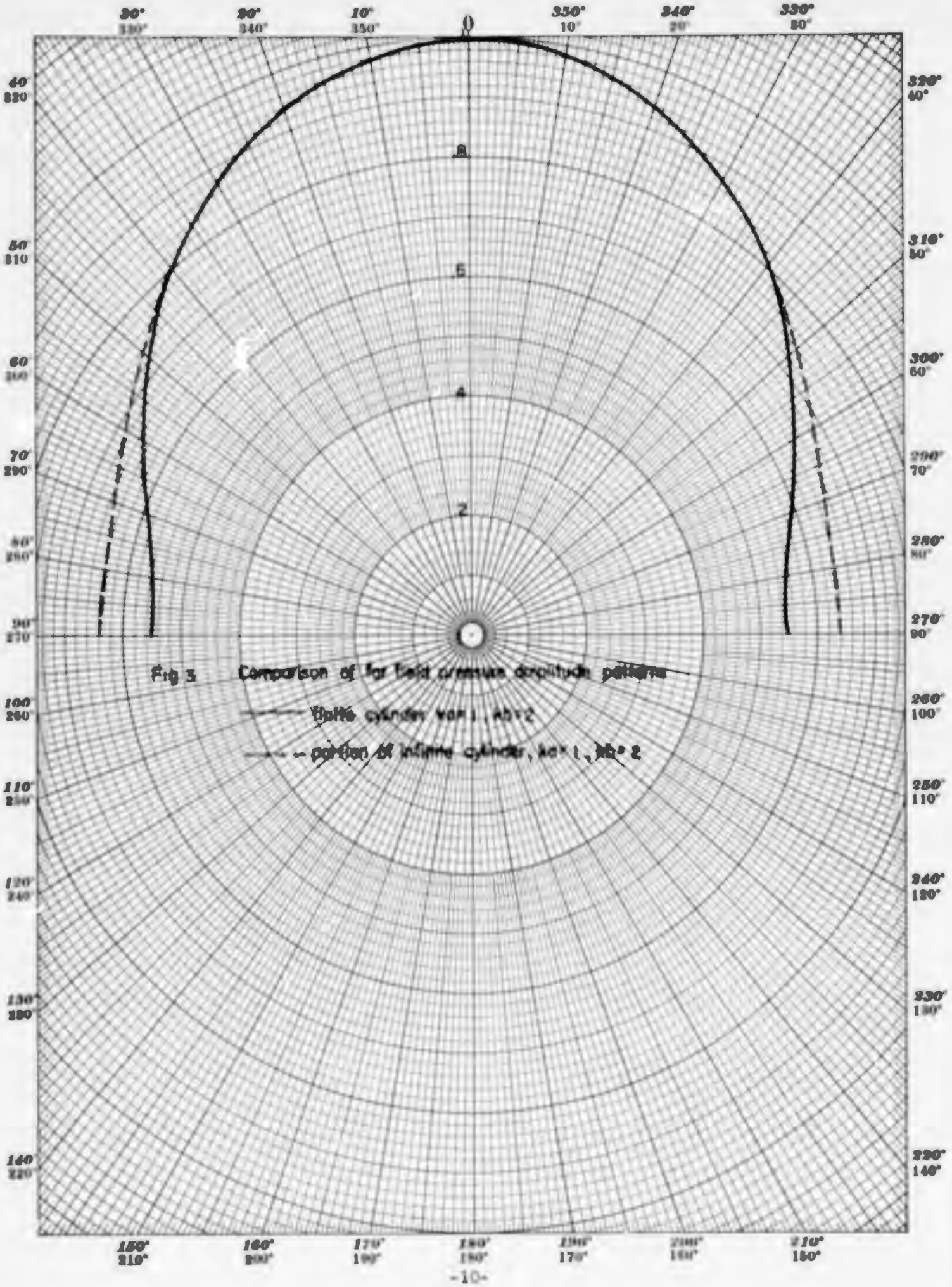

Fig 3 Comparison of far field pressure amplitude patterns

——— Rigid cylinder, $ka = 1$, $kb = 2$

– – – – portion of infinite cylinder, $ka = 1$, $kb = 2$

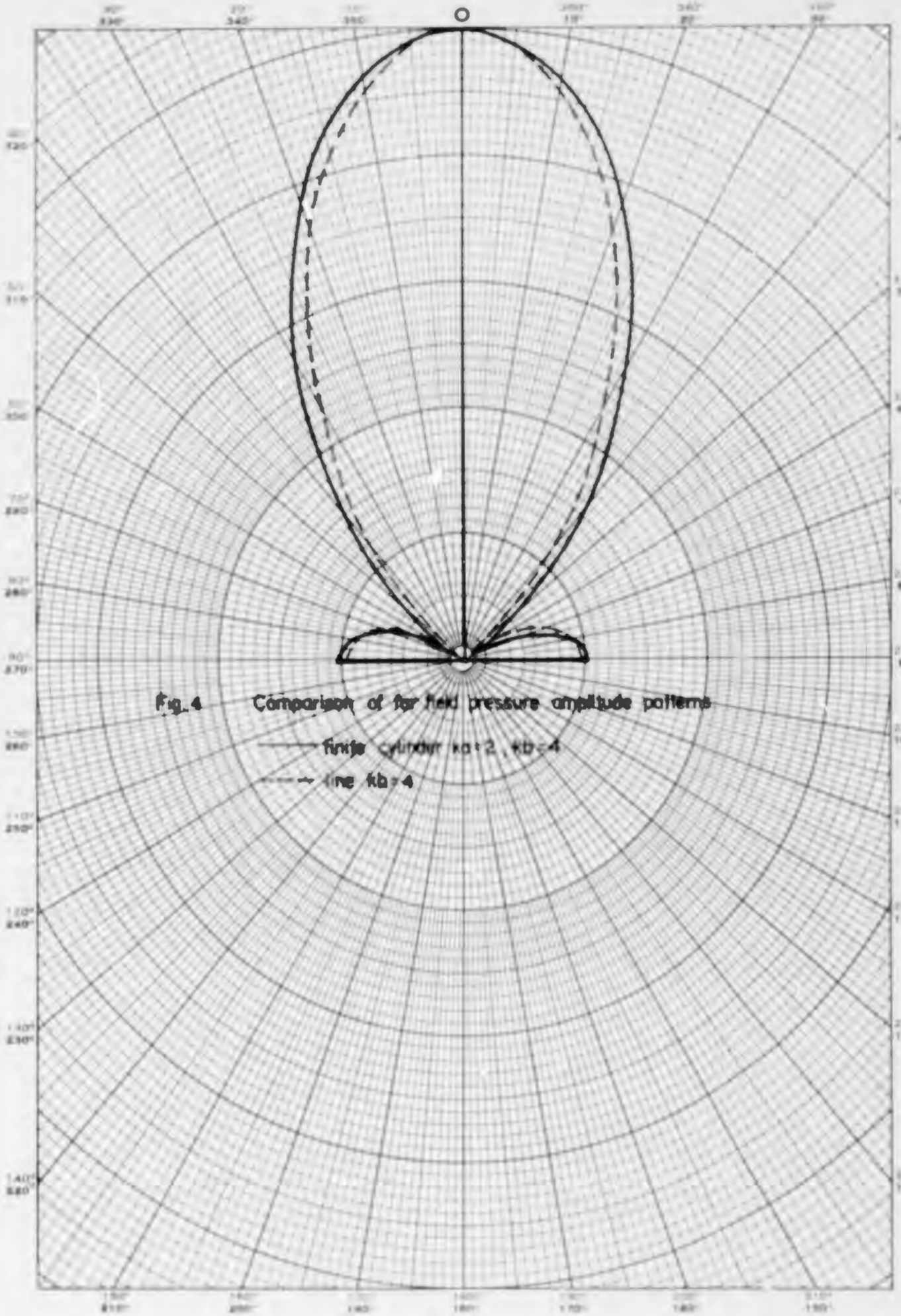

Fig. 4 Comparison of far field pressure amplitude patterns

——— finite cylinder $ka = 2$, $kb = 4$

– – – line $kb = 4$

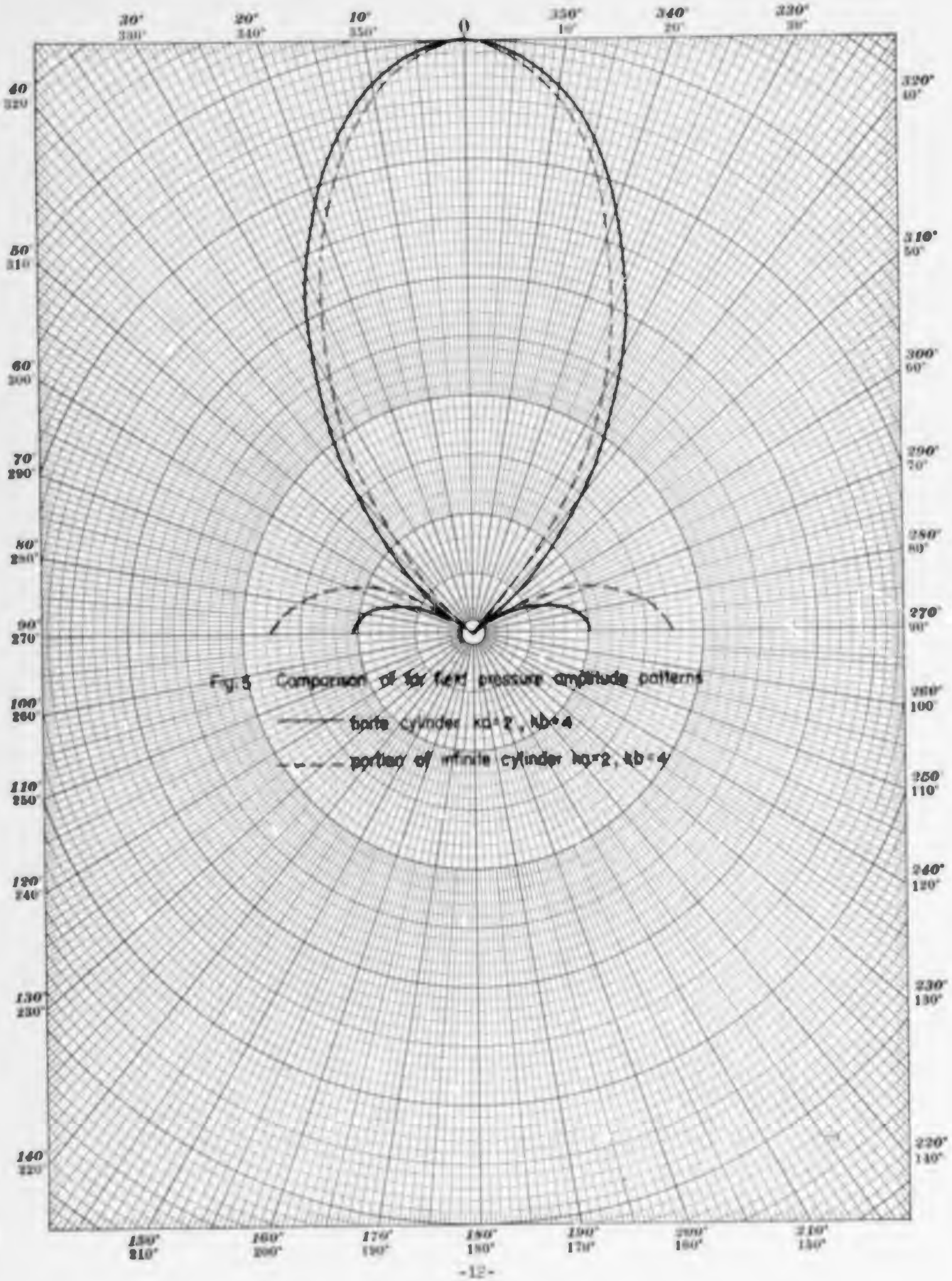

Fig. 5 Comparison of far field pressure amplitude patterns

——— forte cylinder $ka=2$, $kb=4$

– – – portion of infinite cylinder $ka=2$, $kb=4$

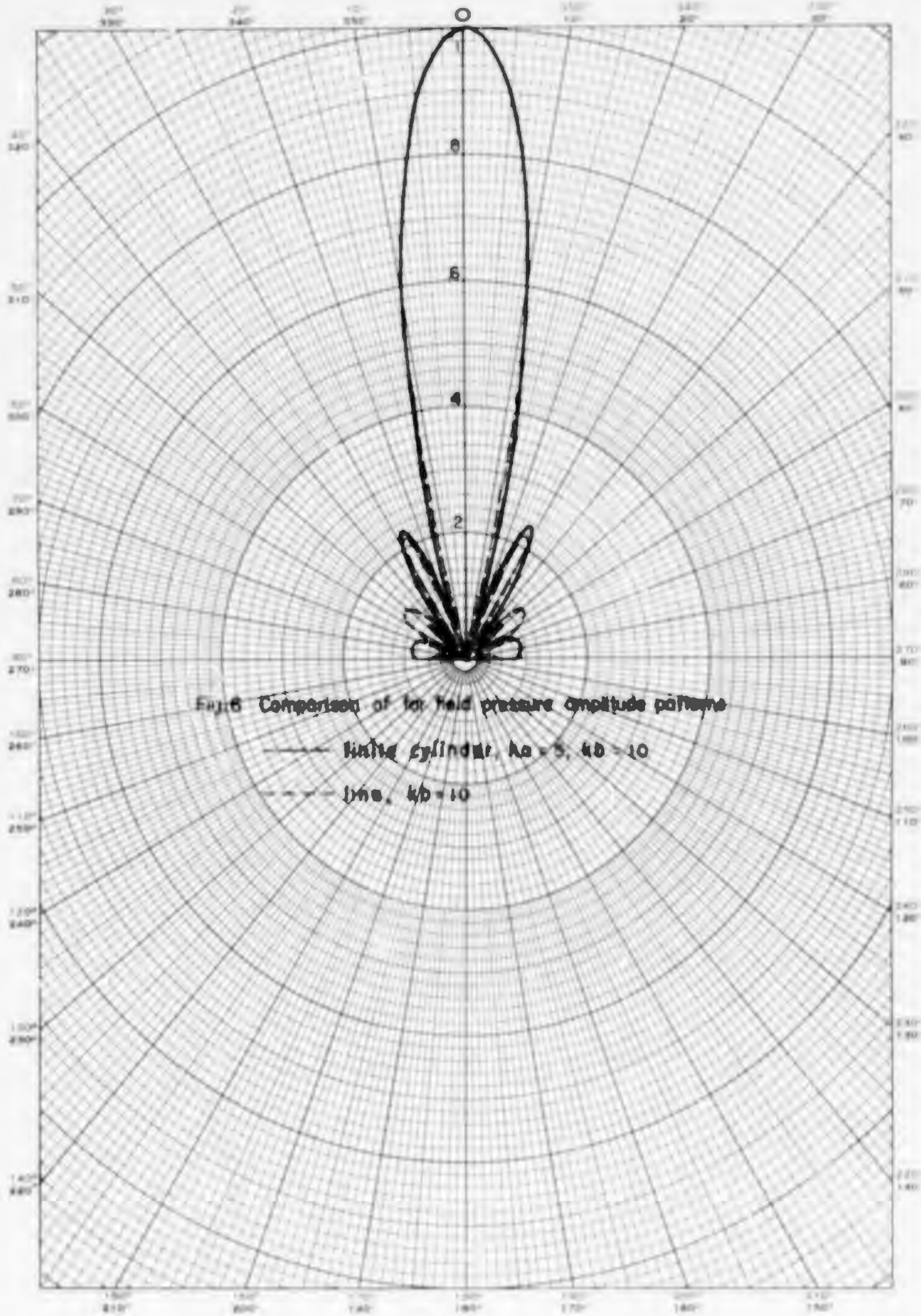

Fig.6 Comparison of far field pressure amplitude patterns

——— finite cylinder, ka = 5, kb = 10

– – – – line, kb = 10

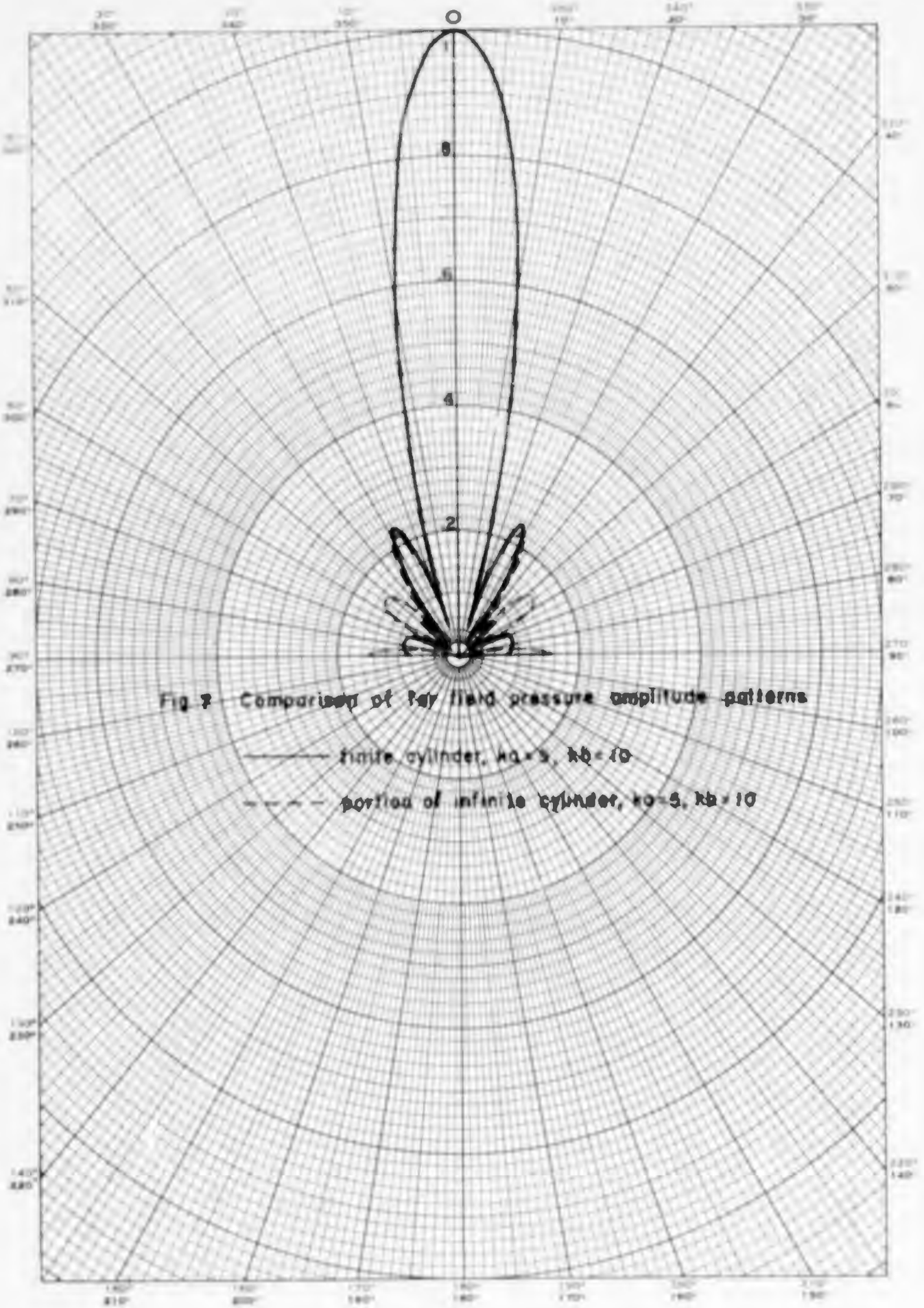

Fig 7 - Comparison of far field pressure amplitude patterns

——— finite cylinder, $ka = 5$, $kb = 10$

– – – – portion of infinite cylinder, $ka = 5$, $kb = 10$

where $H_0^{(1)}$ is the derivative of the cylindrical Hankel function of zero order with respect to its argument. The familiar far field pattern for the line source, in normalized form, is given by

$$p(\theta) = \frac{\sin(kb\cos\theta)}{kb\cos\theta} . \qquad (4)$$

As would be expected the finite cylinder patterns differ from the other patterns used for comparison more and more strongly as the direction of observation approaches the cylinder axis. The comparisons in Figures 3, 5 and 7 show the "end effects" of a finite cylinder radiator. Note that in all three cases the pressure amplitude at $\theta = 0°$ for the finite cylinder lies between the values for the line and for the infinite cylinder.

The finite cylinder amplitude patterns differ from the line and infinite cylinder amplitude patterns by not having zeros. Another aspect of this feature is that the far field phase patterns for the finite cylinder vary continuously with angle, while for the line and infinite cylinder they have a 180 degree discontinuity at each zero of the amplitude pattern. The phase of the sum in Eqn.(2) and of the functions of θ in Eqn.(3) can be directly compared. This is done in Fig.8 for $kb = 1$ and 2 and in Fig.9 for $kb = 5$. We see that near $\theta = 90°$ the two are nearly in phase, but that as the observation direction moves toward the cylinder axis the phase difference increases. Where the infinite cylinder phase pattern has a discontinuity the finite cylinder phase pattern is continuous but varies rapidly with angle.

For the line source the pressure has the same phase throughout each

Fig. 8 Comparison of Far Field Pressure Phase Patterns

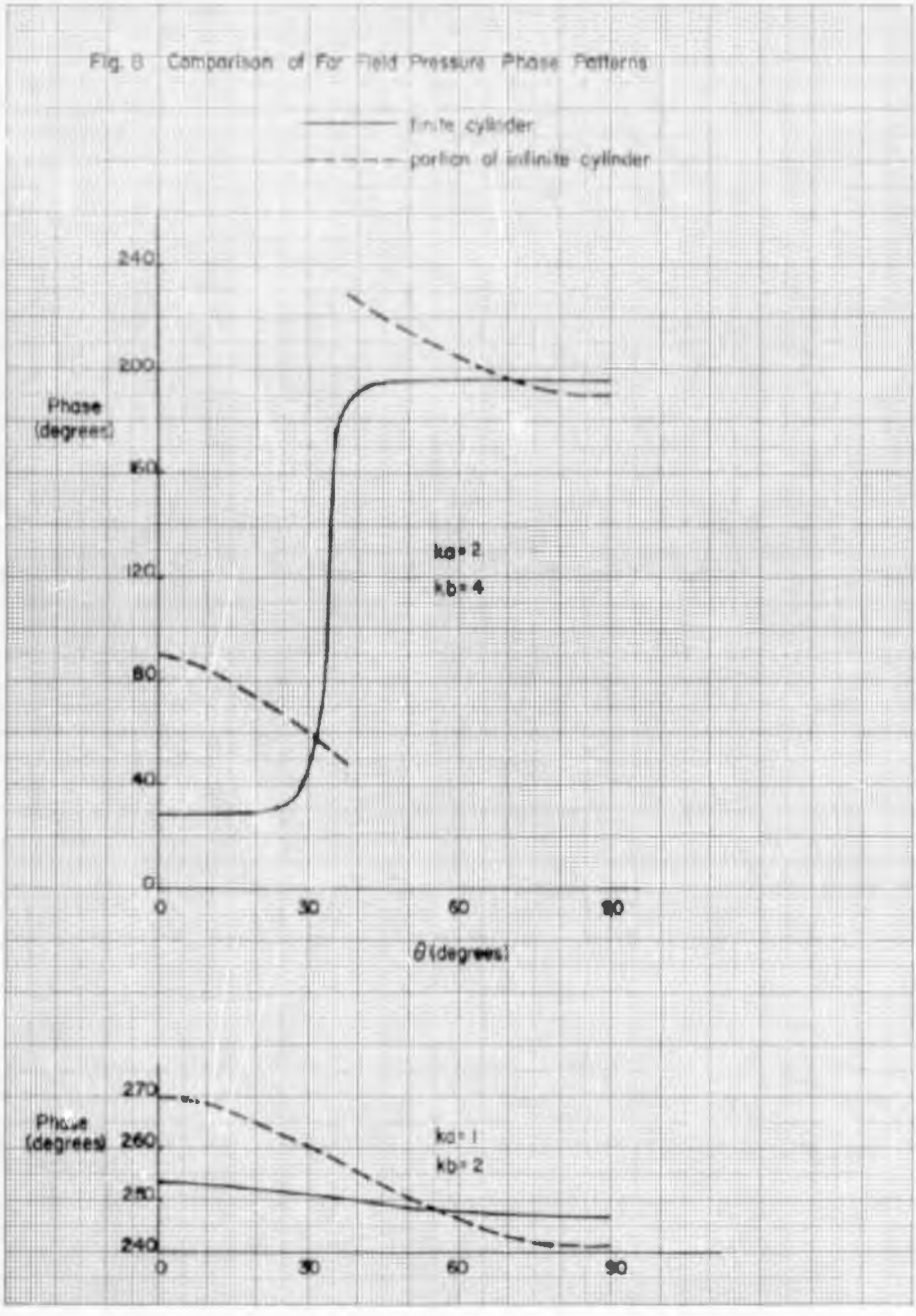

Fig 9 Comparison of Far Field Pressure Phase Patterns

——— finite cylinder

– – – – portion of infinite cylinder

ka = 5

kb = 10

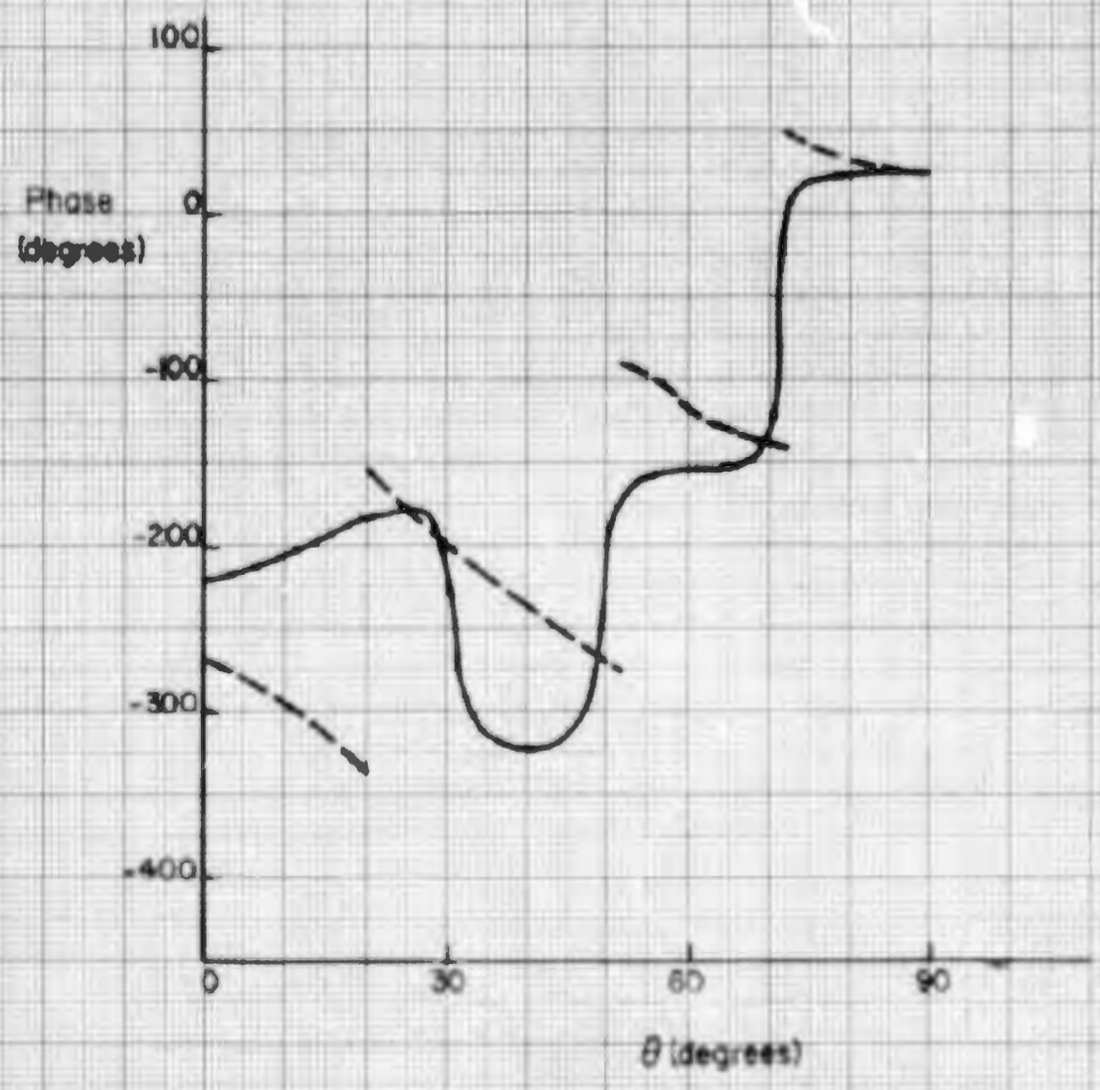

lobe, and the pressure phase pattern consists of constant phase regions separated by 180 degree discontinuities. The finite cylinder phase patterns for $ka=1$ and $ka=2$ correspond closely to this behaviour. However, for $ka=5$, where the minor lobe structure is complicated, this correspondence is obscured beyond the first minor lobe.

Figures 2-9 give the basic results on acoustic radiation from a finite cylinder which have been obtained at this time. In a later section we will derive results on radiation resistance and directivity index from the far field patterns, but we want first to show the degree to which convergence with respect to N has been achieved. For this purpose we have calculated the magnitude and the phase of the sum in Eqn.(2) at $\theta = 90^\circ$ and $\theta = 0^\circ$ as a function of N. The results (unnormalized) are given in Table 4.

The far field results appear to be accurate to about 2% at $\theta = 90^\circ$ (peak of major lobe) but considerably less accurate at $\theta = 0^\circ$. The case $ka=5$ with several values of N is the most illuminating. At $\theta = 0^\circ$ the differences between the magnitudes and phases for successive values of N do not steadily decrease as at $\theta = 90^\circ$, thus leaving the results in doubt. The general picture indicated by Table 4 is that on the major lobe where all terms in the sum add we have greater accuracy, whereas in the minor lobe structure, which is determined by differences among the terms, we have lesser accuracy. Near the minima of the amplitude pattern we could expect the least accuracy. The quantity N_{max}/kb has the values 2,3,4 for $kb = 10, 4, 2$ respectively. It might be expected, therefore, that convergence with respect to N would improve consistently in the order $kb = 10, 4, 2$. However, this

Table 4

Illustration of Convergence with Respect to N

$k_a = 5$ $k_b = 10$

N	$\theta = 0°$ Magnitude	$\theta = 0°$ Phase	$\theta = 90°$ Magnitude	$\theta = 90°$ Phase
10	.8489	185°	3.0300	25°
12	.8092	184°	3.1581	25°
14	.6656	179°	3.2591	25°
16	.5056	170°	3.3420	25°
18	.3820	155°	3.4089	25°
20	.2970	141°	3.4589	25°
		$k_a = 2$	$k_b = 4$	
10	.4148	25°	2.0311	195°
12	.4141	29°	2.0316	195°
		$k_a = 1$	$k_b = 2$	
6	.7476	252°	1.2957	247°
8	.7226	253°	1.3179	246°

is not apparent from the available results, since $kb = 4$ shows the best convergence. This can also be seen in Tables 2 and 3 where convergence of the a_n with N for low n is more complete for $kb = 4$ than for $kb = 2$.

In the far field calculations the last few terms of the sums are negligible, and the last few coefficients (which we do not know accurately) are not required. It must be emphasized, however, that to calculate certain physical results we need to use a certain value of N, not because we need $N/2 + 1$ terms in the expansion, but in order to get stable coefficients for n considerably less than N, the value of N required depending on the physical results to be calculated. Far field results of practically useful accuracy appear to require a value of N at least equal to $2kb$ for $b/a = 2$. Near field results would require larger values of N than we have obtained at this time.

Radiation Resistance and Directivity Index

The time average radiated acoustic power can be easily calculated from the far field pressure amplitudes which have been given previously. The result can be expressed most meaningfully in terms of the radiation resistance. From the power and the previously calculated patterns we can also find the directivity index.

In the far field the time average intensity is

$$I(\theta) = \frac{pp^*}{2\rho c}, \qquad (5)$$

and the power radiated is given by

$$P = \int_0^{2\pi}\int_0^{\pi} I(\theta) r^2 \sin\theta \, d\theta \, d\varphi = \frac{\pi r^2}{\rho c}\int_0^{\pi} p p^* \sin\theta \, d\theta. \tag{6}$$

Using Eqn.(2) we have

$$P = \pi \rho c a^2 U^2 \int_0^{\pi} \left| \sum_{n=0}^{N} \frac{a_n}{aU} i^{-n} P_n(\cos\theta) \right|^2 \sin\theta \, d\theta. \tag{7}$$

The radiation resistance, R, is defined in this case by

$$P = \frac{1}{2} R U^2, \tag{8}$$

and the active area of the source is

$$A = 2\pi a (2b) = 8\pi a^2, \tag{9}$$

since $b = 2a$ in the present cases. Thus we have

$$\frac{R}{\rho c A} = \frac{1}{4}\int_0^{\pi} \left| \sum_{n=0}^{N} \frac{a_n}{aU} i^{-n} P_n(\cos\theta) \right|^2 \sin\theta \, d\theta. \tag{10}$$

The integral in Eqn.(10) was evaluated numerically for the three finite cylinder cases, and the corresponding calculation was done for the band source on the infinite cylinder using Eqn.(3). The results are given in Table 5. We see that the lack of an infinite cylindrical baffle lowers the radiation resistance of a radially pulsating cylinder.

The directivity ratio is defined as the ratio of the maximum intensity, which here occurs in the direction $\theta = 90^\circ$, to the intensity averaged over all directions. The average intensity is equal to the total radiated power divided by the surface area of a sphere in the far field. Thus we have

using Eqn.(5):

$$DR \equiv \frac{I_{max}}{I_{avg}} = \frac{|p(90°)|^2/2\rho c}{P/4\pi r^2} \quad . \tag{11}$$

Using Equations (2), (8) and (9) this can be written

$$DR = \frac{\frac{1}{2}\left|\sum_{n=0}^{N} \frac{a_n}{aU} i^{-n} P_n(0)\right|^2}{R/\rho c A} \quad . \tag{12}$$

The directivity ratio can be obtained immediately from Eqn.(12) and the previously calculated quantities. The figure which is commonly used in Sonar applications is the directivity index, defined by:

$$DI = 10 \log_{10} DR. \tag{13}$$

The directivity index for the three finite cylinder cases and the corresponding infinite cylinder cases are shown in Table 5. There is no practically important distinction between the two. For small ka the finite cylinder is slightly more directive than the infinite cylinder, but as ka increases the infinite cylinder becomes slightly more directive than the finite cylinder.

Table 5

Radiation Resistance and Directivity Index for $b/a = 2$

ka	$R/\rho c A$ finite	$R/\rho c A$ infinite	DI (db) finite	DI (db) infinite
1	.633	.752	1.37	1.27
2	.822	.879	4.00	4.29
5	.944	.978	8.02	8.08

Conclusion

In the past the performance of an actual cylindrical transducer could have been estimated by use of the theoretical results for the infinite cylinder. Table 5 shows that this would overestimate the radiated power, while the directivity index would sometimes be overestimated and sometimes be underestimated. The maximum overestimate of source level (power in db plus directivity index) indicated by the cases in Table 5 is for $ka = 1$ where it would be about 0.7 db. Such errors are not of much significance in transducer design estimates. But it is important to know that the error is not greater than this, which the present finite cylinder calculations demonstrate, probably for the first time. The differences in the minor lobe structure for the cylindrical source with and without the infinite cylindrical baffle may also not be of practical significance, although such questions must be considered individually for each application.

The results presented here have been intended mainly to demonstrate the feasibility of the method of calculation described in reference 1. In the following paragraphs we mention other interesting problems for which calculations could be made, as well as some of the ways in which the method could be improved.

In this method of solving the finite cylinder problem it would seem appropriate to use prolate spheroidal coordinates (and the corresponding wave functions) for $b/a > 1$, oblate spheroidal coordinates for $b/a < 1$, and spherical coordinates only for $b/a = 1$. However, the relative simplicity of the spherical wave functions would favor their use for b/a different from

unity, and one of the questions for further study is the range of b/a which it is feasible to handle by use of spherical wave functions.

The present calculations, using spherical wave functions with $b/a = 2$ have provided some results, but have also shown that it is difficult to get the accuracy desired. We could expect that the same amount of computational effort would yield more results for b/a closer to unity. There are various other finite cylinder calculations with b/a not far from unity which would be useful in transducer design. One of the most useful cases is probably that of the cylinder vibrating on one or both ends with the sides rigid. With some improvements in the existing computer program it should be possible to obtain enough coefficients in such cases to permit calculation of the near field and such practically important information as the radiation reactance.

Practical problems involving acoustic sources of other shapes could also be treated by this method. Source shapes which do not differ greatly from a sphere would, of course, be the easiest to handle, and would not tax the capabilities of the method as much as the finite cylinder. For example, the rigid sphere with a vibrating flat spot[7] would serve as a useful model of a transducer in a rigid housing.

References

1) N. G. Parke, W. Williams, "Mathematical Methods in Transducer Field Theory: The Finite Cylinder", Parke Mathematical Laboratories Final Report on Contract N140(70024)72788B, December 1962.

2) M. C. Junger, "Sound Radiation from a Radially Pulsating Cylinder of Finite Length", Harvard University Acoustics Research Laboratory, June 24, 1955.

3) G. A. Brigham, M. F. Borg, JASA, 32 971 (1960)

4) L. H. Chen, D. G. Schweikert, JASA, 35 1626 (1963)

5) G. H. Conant, "Cylindrical Acoustic Radiator Solution (Version A)", Report to Parke Mathematical Laboratories, March 31, 1964.

6) D. J. Laird, H. Cohen, JASA, 24 46 (1952)

7) C. H. Sherman, D. A. Moran, B. T. Howard, "Acoustic Radiation from a Sphere with a Flat Spot", PML Tech. Memo. No. 1 for Hazeltine Corp., January 1964.(This memorandum describes the first stages of the solution and does not include final results.)